哈爾濱工業大學
HARBIN INSTITUTE OF TECHNOLOGY

AI and big data for energy systems

Name: Bai Mingliang

Institution: Harbin Institute of Technology

Date: 2024.02.20

1 AI for renewable energy forecast

2 AI for fault diagnosis of energy systems

Significance of AI-based renewable energy forecast

- Developing renewable energy is crucial to tackling climate change.
- According to IEA, solar PV claims the most installed power capacity worldwide by 2027, surpassing coal, natural gas and hydropower.
- Wind and Solar power has strong uncertainties and harms the stability of the electricity grid.
- Accurate wind and solar power forecast is crucial in the electricity grid.
- Deep learning is the breakthrough of AI technology and has promising applications in renewable energy forecast

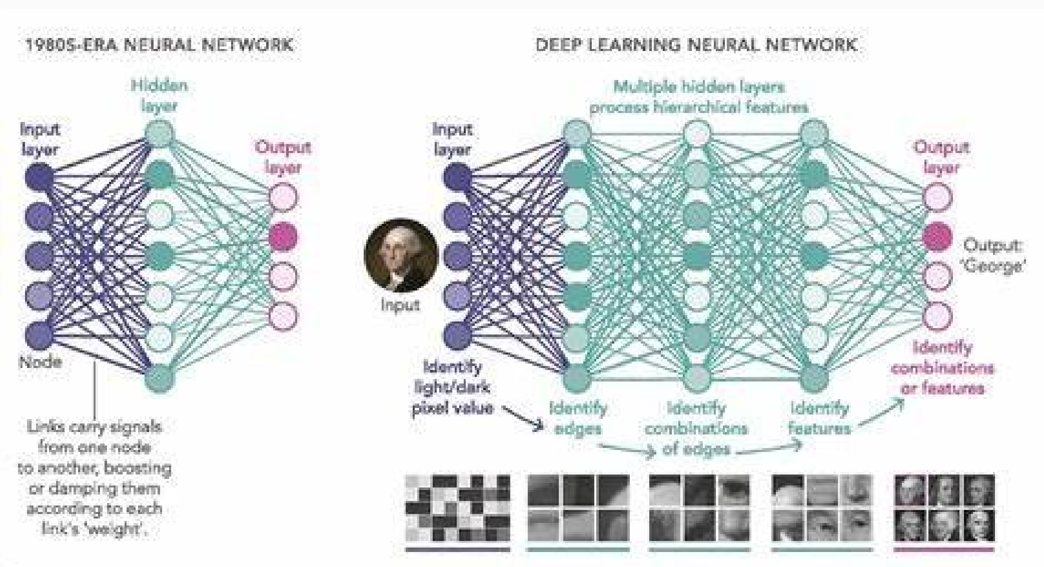

Feature selection in renewable energy forecast

- There are many related variables in forecast, and selecting the important variables for forecast is necessary.
- Propose a new information gain factor η for adding the new feature a in forecast.
- Larger information gain factor correpsonds to larger forest error reduction.

$$\eta = \frac{p\left[X_{(GHI,a)_{t-1}}, Y_{GHI_t}\right] - p\left[X_{GHI_{t-1}}, Y_{GHI_t}\right]}{1 - p\left[X_{GHI_{t-1}}, Y_{GHI_t}\right]} \times 100\%$$

$$p_{X,Y} = \frac{\sum_{i=1}^{n}(X_i - \overline{X})(Y_i - \overline{Y})}{\sqrt{\sum_{i=1}^{n}(X_i - \overline{X})^2}\sqrt{\sum_{i=1}^{n}(Y_i - \overline{Y})^2}}$$

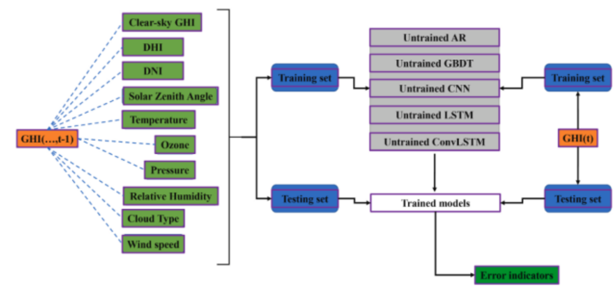

Fig. 1. The process of the forecasting experiment.

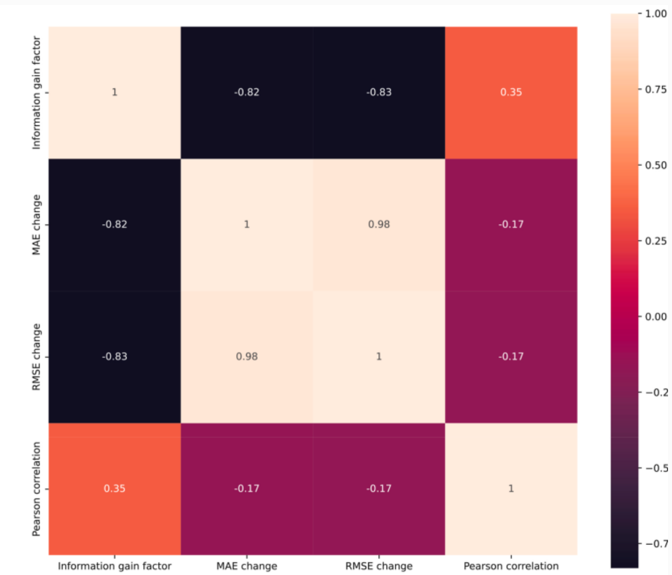

Fig. 19. Correction between error changes and information gain factor.

Sort of error reduction and information gain.

Sort	δ_a MAE/NMAE	δ_a RMSE/NRMSE	η
1	Clear-sky GHI −16.83%	Clear-sky GHI −7.12%	Clear-sky GHI 4.593%
2	Solar zenith angle −6.33%	Solar zenith angle −3.88%	Solar zenith angle 0.722%
3	Relative humidity −4.38%	Temperature −2.86%	Wind speed 0.254%
4	Temperature −4.25%	Relative humidity −1.77%	Relative humidity 0.133%
5	Pressure −1.36%	DNI −1.30%	Temperature 0.055%
6	Wind speed −0.99%	Wind speed −0.92%	Pressure 0.049%
7	DNI −0.61%	Pressure −0.40%	DNI 0.042%
8	DHI 2.81%	Ozone −0.02%	DHI 0.021%
9	Ozone 3.38%	DHI 0.39%	Cloud type 0.001%
10	Cloud type 8.41%	Cloud type 1.64%	Ozone 0.000%

Chen Y, **Bai M**, Zhang Y, et al. Proactively selection of input variables based on information gain factors for deep learning models in short-term solar irradiance forecasting[J]. Energy, 2023, 284: 129261.

Attention ConvLSTM-based multivariable fusion in forecast

- PV power generation aims to convert solar energy to electricity. The PV power output is affected by **solar irradiance**, **temperature** etc. Thus, it is necessary to use these variables in PV forecast.

$$P_s = \frac{H_s}{H_{stc}} * P_{stc} * c_1 * [1 + c_2 * (T_s - T_{stc})]$$

- Clear-sky GHI characterize the solar irradiance under cloudless situation, and is often used as the physical prior knowledge in PV forecast.

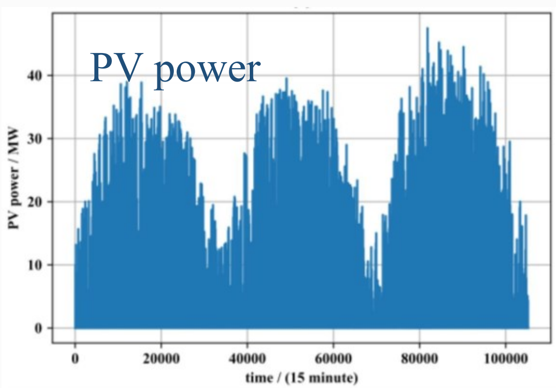

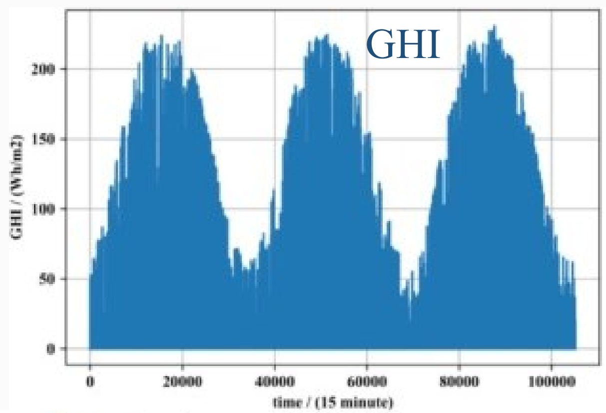

clear-sky GHI

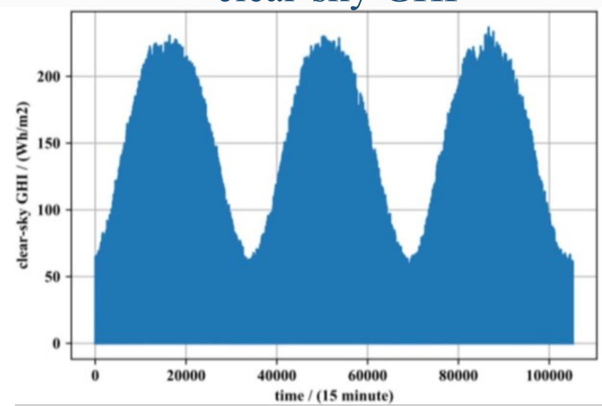

Clear-sky index

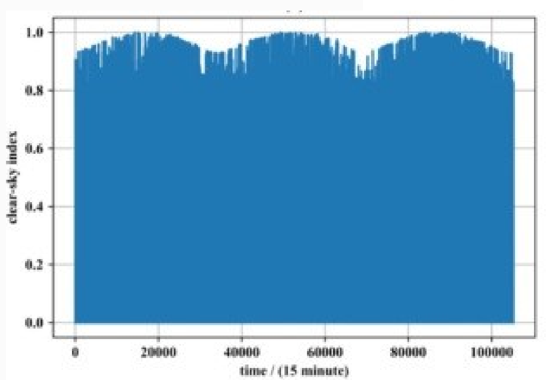

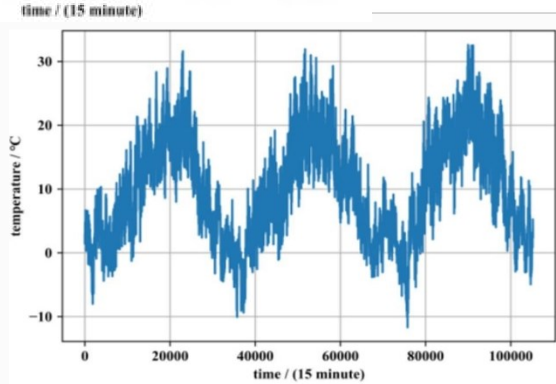

Air temperature

Bai, Mingliang, et al. "Deep attention ConvLSTM-based adaptive fusion of clear-sky physical prior knowledge and multivariable historical information for probabilistic prediction of photovoltaic power." Expert Systems with Applications 202 (2022): 117335.

Attention ConvLSTM-based multivariable fusion in forecast

- ConvLSTM is used to extract the information from multiple variables related to PV power and the temporal information from historical PV data.
- Attention mechanism imitates the brain of people. People usually focus on important things, while the attention mechanism can help the neural network to assign larger weights for important features.
- Attention mechanism is used to adaptively assign different weights for clear-sky prior knowledge and various historical variables.

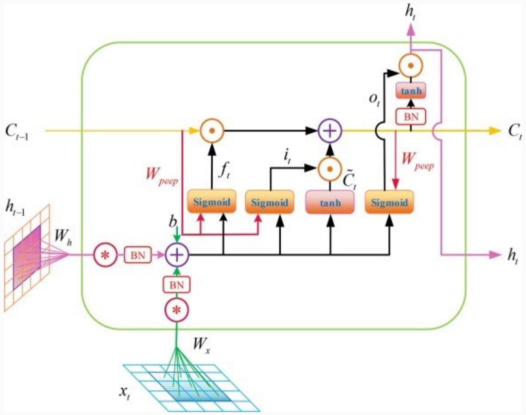

$$a_t(s) = \frac{\exp(\mathrm{score}(h_t, \bar{h}_s))}{\sum_{s'} \exp(\mathrm{score}(h_t, \bar{h}_{s'}))}$$

$$\mathrm{score}(h_t, \bar{h}_s) = h_t^T \mathbf{W_a} \bar{h}_s$$

$$c_t = \sum_s a_t(s) \cdot \bar{h}_s$$

$$\tilde{h}_t = \tanh(W_c \cdot [c_t, h_t])$$

$$y_t = W_o \tilde{h}_t + b_o$$

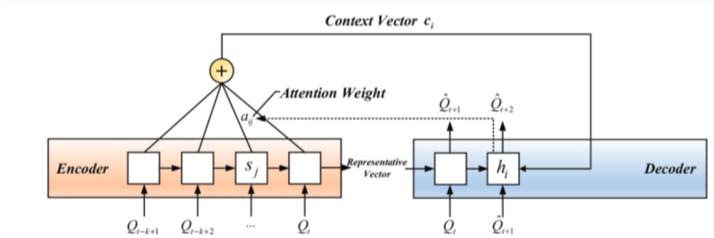

Fig. 6. Attention mechanism.

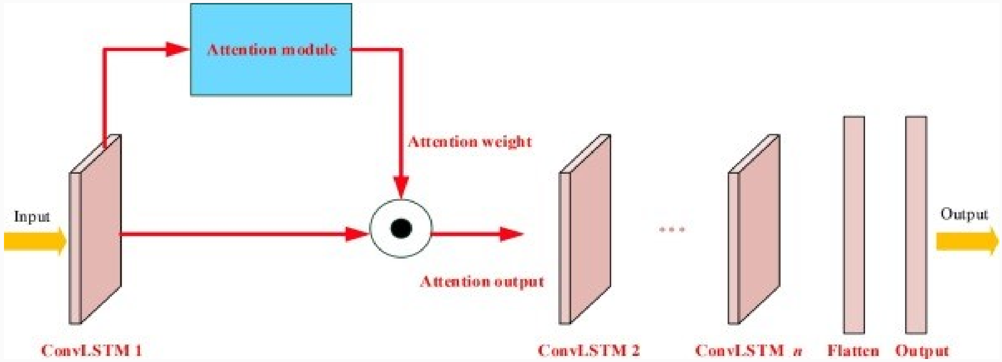

Bai, Mingliang, et al. "Deep attention ConvLSTM-based adaptive fusion of clear-sky physical prior knowledge and multivariable historical information for probabilistic prediction of photovoltaic power." Expert Systems with Applications 202 (2022): 117335.

Attention ConvLSTM-based multivariable fusion in forecast

- Two years' data (2016-2017) are used to train attention CNN.
- Data from the year 2018 is used as the test set to evaluate the forecast performance.

Table 4
Comparison between Attention ConvLSTM and other methods in Brussels dataset (unit: MW).

		1-step	2-step	3-step	4-step
Naive Persistence	MAE	0.8480	1.2685	1.6900	2.1111
	RMSE	2.3383	2.9519	3.5771	4.2165
	WMAPE	0.1496	0.2238	0.2981	0.3724
	nRMSE	0.0481	0.0608	0.0736	0.0868
SVR	MAE	1.0793	1.4946	1.8263	2.1301
	RMSE	2.2569	2.7758	3.2033	3.5860
	WMAPE	0.1904	0.2637	0.3222	0.3758
	nRMSE	0.0464	0.0571	0.0659	0.0738
ELM	MAE	0.7975	1.0290	1.2379	1.4327
	RMSE	2.1994	2.6013	2.9520	3.2647
	WMAPE	0.1407	0.1815	0.2184	0.2527
	nRMSE	0.0453	0.0535	0.0608	0.0672
CART	MAE	0.8235	1.0830	1.3416	1.6009
	RMSE	2.4534	2.8824	3.2529	3.6142
	WMAPE	0.1453	0.1911	0.2367	0.2824
	nRMSE	0.0505	0.0593	0.0669	0.0744
GBDT	MAE	0.7544	0.9798	1.1821	1.3688
	RMSE	2.1823	2.5338	2.8539	3.1522
	WMAPE	0.1331	0.1728	0.2085	0.2415
	nRMSE	0.0449	0.0521	0.0587	0.0649
CNN	MAE	0.7920	0.9767	1.1321	1.4043
	RMSE	2.1720	2.4781	2.6773	2.9251
	WMAPE	0.1395	0.1724	0.1997	0.2474
	nRMSE	0.0447	0.0510	0.0551	0.0602
LSTM	MAE	0.8534	0.9767	1.1079	1.3362
	RMSE	2.1396	2.4732	2.6676	2.9348
	WMAPE	0.1505	0.1722	0.1954	0.2357
	nRMSE	0.0440	0.0509	0.0549	0.0604
ARIMAX	MAE	0.7552	1.0326	1.2835	1.5203
	RMSE	2.2221	2.6253	2.9785	3.3043
	WMAPE	0.1335	0.1826	0.2269	0.2688
	nRMSE	0.0457	0.0540	0.0613	0.0680
Attention ConvLSTM	MAE	0.7143	0.8698	0.9864	1.0884
	RMSE	2.0797	2.3615	2.5607	2.7210
	WMAPE	0.1259	0.1533	0.1743	0.1919
	nRMSE	0.0428	0.0486	0.0527	0.0560

Table 5
Comparison between Attention ConvLSTM and other methods in Luxembourg Province (unit: MW).

		1-step	2-step	3-step	4-step
Naive Persistence	MAE	1.8541	2.4898	3.1847	3.8499
	RMSE	4.7532	5.6548	6.6997	7.6836
	WMAPE	0.1829	0.2456	0.3141	0.3797
	nRMSE	0.0553	0.0658	0.0779	0.0894
SVR	MAE	2.3872	3.0325	3.5921	4.1301
	RMSE	4.5206	5.3411	6.0714	6.7349
	WMAPE	0.2354	0.2991	0.3543	0.4073
	nRMSE	0.0526	0.0621	0.0706	0.0783
ELM	MAE	1.7649	2.1254	2.4675	2.7639
	RMSE	4.3547	5.0041	5.6008	6.0506
	WMAPE	0.1741	0.2096	0.2434	0.2726
	nRMSE	0.0507	0.0582	0.0652	0.0704
CART	MAE	1.8021	2.2403	2.7254	3.2251
	RMSE	4.6777	5.3898	6.1322	6.8592
	WMAPE	0.1777	0.2210	0.2688	0.3181
	nRMSE	0.0544	0.0627	0.0713	0.0798
GBDT	MAE	1.7245	2.0944	2.4485	2.7510
	RMSE	4.3135	4.9066	5.4642	5.9196
	WMAPE	0.1701	0.2066	0.2415	0.2713
	nRMSE	0.0502	0.0571	0.0636	0.0689
CNN	MAE	1.7364	2.1490	2.3467	2.7249
	RMSE	4.2980	4.8739	5.3553	5.7249
	WMAPE	0.1712	0.2123	0.2315	0.2684
	nRMSE	0.0500	0.0567	0.0623	0.0666
LSTM	MAE	1.8670	2.2006	2.3983	2.6905
	RMSE	4.4420	4.9513	5.4842	5.7937
	WMAPE	0.1841	0.2169	0.2361	0.2655
	nRMSE	0.0517	0.0576	0.0638	0.0674
ARIMAX	MAE	1.7361	2.1795	2.6340	3.0348
	RMSE	4.6331	5.2623	5.9496	6.5098
	WMAPE	0.1716	0.2155	0.2604	0.3000
	nRMSE	0.0539	0.0612	0.0692	0.0757
Attention ConvLSTM	MAE	1.6590	1.8911	2.1060	2.2522
	RMSE	4.1519	4.6075	4.9943	5.1920
	WMAPE	0.1639	0.1864	0.2077	0.2219
	nRMSE	0.0483	0.0536	0.0581	0.0604

$$MAE = \frac{1}{n}\sum_{i=1}^{n}|y_i - \hat{y}_i|$$

$$RMSE = \sqrt{\frac{1}{n}\sum_{i=1}^{n}(y_i - \hat{y}_i)^2}$$

$$nRMSE = \frac{\mathrm{RMSE}}{y_{\mathrm{rated}}}$$

$$WMAPE = \frac{\sum_{i=1}^{n}|y_i - \hat{y}_i|}{\sum_{i=1}^{n} y_i}$$

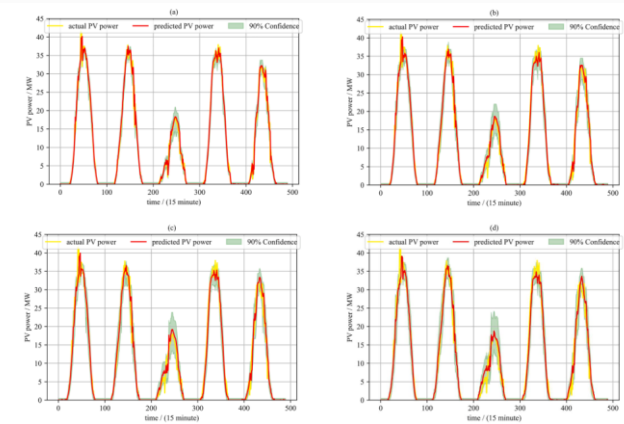

Fig. 21. Probabilistic interval forecast for Brussels dataset in (a) 1-step prediction, (b) 2-step prediction, (c) 3-step prediction and (d) 4-step prediction.

Bai, Mingliang, et al. "Deep attention ConvLSTM-based adaptive fusion of clear-sky physical prior knowledge and multivariable historical information for probabilistic prediction of photovoltaic power." Expert Systems with Applications 202 (2022): 117335.

Post-processing NWP for 4-hour-ahead PV forecast

- Forecast errors usually increases with the lead time for purely data-driven forecast methods. Long-range forecast usually relies on Numerical Weather Prediction (NWP).
- NWP solves partial difference equations of atmosphere. Due to the influence of inaccurate initial conditions, model resolution, model biases etc., NWP has errors in weather forecast and it's necessary to perform NWP error correction.

Table 6 Comparison between the proposed method and conventional forecast methods for 1–4 step prediction

		1-step	2-step	3-step	4-step
Naive Persistence	nMAE	0.0175	0.0261	0.0348	0.0434
	nRMSE	0.0481	0.0608	0.0736	0.0868
CART	nMAE	0.0182	0.0248	0.0324	0.0405
	nRMSE	0.0474	0.0581	0.0698	0.0822
ELM	nMAE	0.0172	0.0226	0.0274	0.0316
	nRMSE	0.0452	0.0540	0.0615	0.0683
Extra tree	nMAE	0.0190	0.0244	0.0292	0.0327
	nRMSE	0.0540	0.0637	0.0719	0.0776
GBDT	nMAE	0.0166	0.0215	0.0259	0.0298
	nRMSE	0.0441	0.0517	0.0585	0.0646
XGBoost	nMAE	0.0153	0.0196	0.0231	0.0261
	nRMSE	0.0440	0.0524	0.0582	0.0634
LightGBM	nMAE	0.0161	0.0209	0.0252	0.0290
	nRMSE	0.0433	0.0512	0.0581	0.0643
Random Forecast	nMAE	0.0149	0.0193	0.0228	0.0259
	nRMSE	0.0439	0.0519	0.0577	0.0628
SVR	nMAE	0.0308	0.0442	0.0545	0.0638
	nRMSE	0.0493	0.0624	0.0731	0.0826
Proposed method	nMAE	**0.0137**	**0.0167**	**0.0187**	**0.0198**
	nRMSE	**0.0425**	**0.0481**	**0.0512**	**0.0540**

Table 9 Comparison between the proposed method and conventional forecast methods for 13–16 step prediction

		13-step	14-step	15-step	16-step
Naive Persistence	nMAE	0.1080	0.1146	0.1211	0.1274
	nRMSE	0.1795	0.1887	0.1977	0.2062
CART	nMAE	0.1032	0.1097	0.1161	0.1223
	nRMSE	0.1733	0.1825	0.1916	0.2001
ELM	nMAE	0.0480	0.0490	0.0499	0.0506
	nRMSE	0.0893	0.0908	0.0921	0.0934
Extra tree	nMAE	0.0478	0.0486	0.0495	0.0503
	nRMSE	0.1003	0.1020	0.1036	0.1051
GBDT	nMAE	0.0469	0.0478	0.0487	0.0494
	nRMSE	0.0910	0.0927	0.0944	0.0959
XGBoost	nMAE	0.0387	0.0397	0.0406	0.0413
	nRMSE	0.0813	0.0830	0.0846	0.0860
LightGBM	nMAE	0.0463	0.0474	0.0484	0.0493
	nRMSE	0.0910	0.0931	0.0949	0.0966
Random Forecast	nMAE	0.0394	0.0403	0.0411	0.0418
	nRMSE	0.0835	0.0852	0.0866	0.0878
SVR	nMAE	0.1002	0.1018	0.1033	0.1041
	nRMSE	0.1197	0.1215	0.1233	0.1243
Proposed method	nMAE	**0.0252**	**0.0253**	**0.0255**	**0.0258**
	nRMSE	**0.0607**	**0.0610**	**0.0615**	**0.0617**

$$\mathrm{nMAE} = \frac{1}{n y_{\mathrm{rated}}} \sum_{i=1}^{n} |y_i - \hat{y}_i|$$

$$\mathrm{nRMSE} = \frac{1}{y_{\mathrm{rated}}} \sqrt{\frac{1}{n} \sum_{i=1}^{n} (y_i - \hat{y}_i)^2}$$

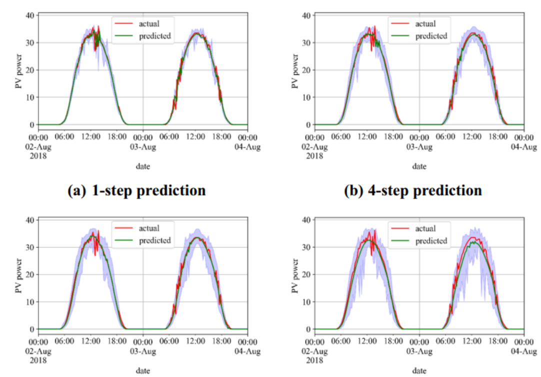

(a) 1-step prediction (b) 4-step prediction

(c) 8-step prediction (d) 16-step prediction

Bai Mingliang, Zhou Zhihao, Chen Yunxiao, Liu Jinfu, Yu Daren. Accurate four-hour-ahead probabilistic forecast of photovoltaic power generation based on multiple meteorological variables-aided intelligent optimization of numeric weather prediction data[J]. Earth Science Informatics.

Error revision during morning period for solar forecast without NWP

- Numerical Weather Prediction (NWP) are often hard to obtain for ordinary PV users, like the users of rooftop PV.
- Error revision during morning period is proposed and the forecast during the rest time of the day is significantly improved.

$$k_i = \frac{y_{\text{action},i}}{y_{\text{prediction},i}}$$

$$y^{\text{revised}}_{\text{prediction},i} = y_{\text{prediction},i} \times \overline{k_i}, (i \geq n+1)$$

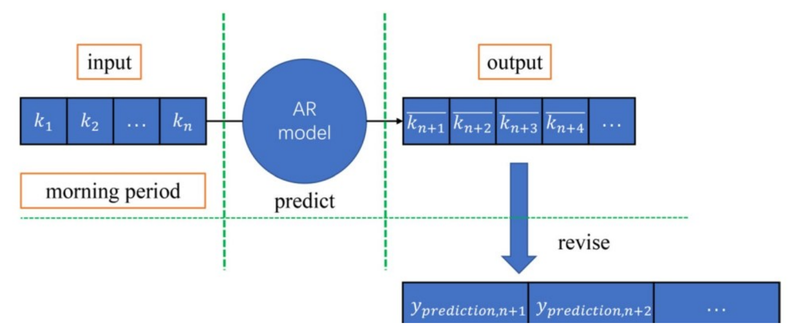

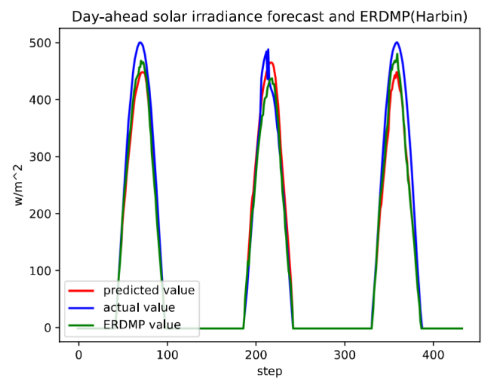

Fig. 19 ERDMP for Harbin (8:00 a.m.)

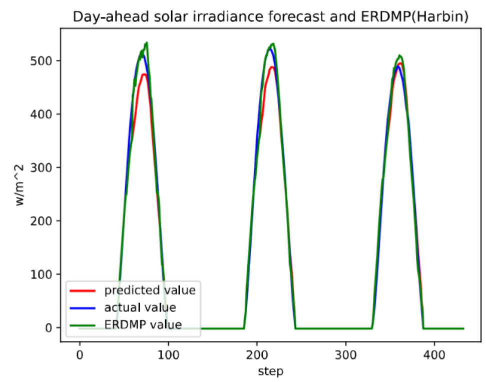

Fig. 21 ERDMP for Harbin (10:00 a.m.)

Table 16 Comparison between ERDMP and other methods (Harbin)

Indicators	RNN_ERDMP	CNN_ERDMP	LSTM_ERDMP	AR	GBDT	ELM	Naive Persistence
MAE	38.342	42.888	**38.245**	54.003	53.822	56.026	56.852
RMSE	83.258	90.713	**82.945**	113.761	111.323	108.472	133.343
R^2	0.884	0.863	**0.885**	0.784	0.793	0.804	0.705

Chen Y, **Bai M**, Zhang Y, et al. Error revision during morning period for deep learning and multi-variable historical data-based day-ahead solar irradiance forecast: towards a more accurate daytime forecast[J]. Earth Science Informatics, 2023: 1-23.

GraphGRU-based joint prediction of multiple PV station

- Conventional PV forecasts are targeted for a single PV station.
- Reveal the spatial correlation and information gain through Moran index, Granger causality test and transfer entropy.
- Propose Graph gated recurrent unit (GraphGRU) network for joint prediction of multiple PV stations, and significantly improves the forecast accuracy of multiple PV stations.

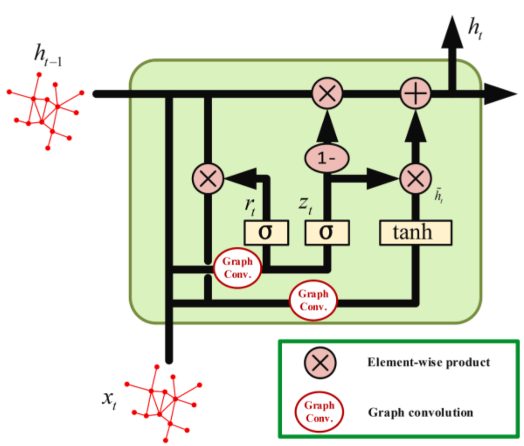

Fig. 4. The proposed Graph Gated Recurrent Unit (GraphGRU) network.

$$z_t = \sigma(\hat{A}\cdot[h_{t-1}, x_t]\cdot W_1 + b_1)$$

$$r_t = \sigma(\hat{A}\cdot[h_{t-1}, x_t]\cdot W_2 + b_2)$$

$$\tilde{h}_t = \tanh(\hat{A}\cdot[r_t \odot h_{t-1}, x_t]\cdot W_3 + b_3)$$

$$h_t = (1 - z_t) \odot h_{t-1} + z_t \odot \tilde{h}_t$$

Fig. 1. Graph structure.

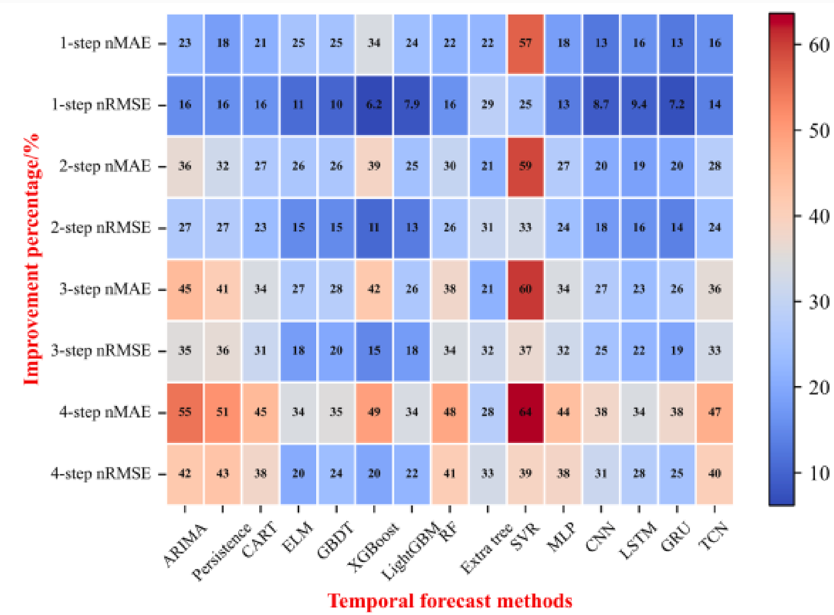

(g) Percentage improvement of the proposed method than conventional temporal methods in Liege Province dataset

Bai Mingliang et al. Deep graph gated recurrent unit network-based spatial-temporal multi-task learning for intelligent information fusion of multiple sites with application in short-term spatial-temporal probabilistic forecast of photovoltaic power[J]. Expert Systems with Applications

Joint prediction of average value, fluctuation scope and change rate

- Wind fluctuation scope and change rate predictions are also highly crucial for dispatching.
- Propose multi-task one-dimensional convolutional neural network for joint prediction of average value, fluctuation scope and change rate.

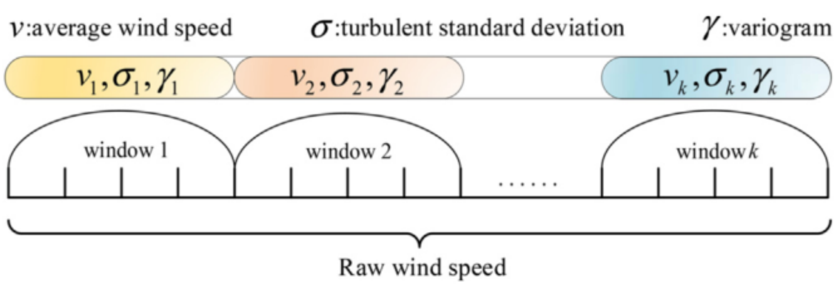

Fig. 1. Windowed downscaling process for multi-parameter of wind.

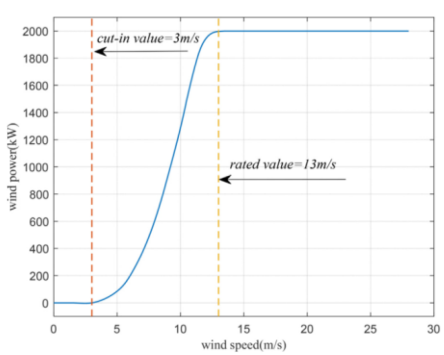

Fig. 8. Wind speed-power curve of the used generator.

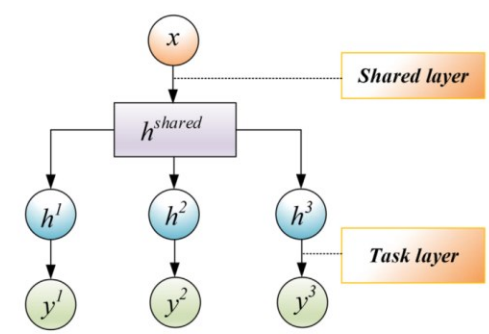

Fig. 2. Structure of multi-task learning model.

(a) RMSE(left) and MAE(right) comparison for 1-step $\{v,\sigma,\gamma^{1/2}\}$ prediction

Zhao, Xinyu, **Mingliang Bai,** Xusheng Yang, Jinfu Liu, Daren Yu, and Juntao Chang. "Short-term probabilistic predictions of wind multi-parameter based on one-dimensional convolutional neural network with attention mechanism and multivariate copula distribution estimation." Energy 234 (2021): 121306.

1 AI for renewable energy forecast

2 AI for fault diagnosis of energy systems

Feature selection in fault diagnosis

- Propose a novel measure of attribute significance with complexity weight for fault diagnosis.
- A novel heuristic attribute reduction algorithm called HSRM-R algorithm is developed, and achieved better performance than conventional methods.

$$SIG_{stru}(a, B, D) = SIG_{stru}(B \cup \{a\}) - SIG_{stru}(B)$$
$$= [\gamma_{B\cup\{a\}}(D) - \gamma_B(D)] - w[\frac{N_R(B\cup\{a\})}{l} - \frac{N_R(B)}{l}],$$

Algorithm: HSRM-R algorithm

Input: $IS = < U, A = C \cup D, V, f >$ and a weight coefficient $w \in [0, +\infty)$

Output: One reduct B and one rule set $\mathbb{T}$

Step 1: $B \leftarrow \varnothing$; // B is the pool to contain the selected attributes.

$\mathbb{T} \leftarrow \varnothing$; // $\mathbb{T}$ is the pool to contain the extracted rules.

Step 2: **for** each $a_i \in C - B$

Extract rules from set B and obtain rule set $\mathbb{T}$ as well as the number of rules;

Extract rules from set $B \cup \{a_i\}$ and obtain the number of rules $N_R(B \cup \{a_i\})$;

Compute $SIG_{stru}(a_i, B, D)$ using the following equation:

$$SIG_{stru}(a_i, B, D) = [\gamma_{B\cup\{a_i\}}(D) - \gamma_B(D)] - w[\frac{N_R(B\cup\{a_i\})}{l} - \frac{N_R(B)}{l}];$$

end

Step 3: Select the attribute a_k which satisfies:

$SIG_{stru}(a_k, B, D) = \max_i(SIG_{stru}(a_i, B, D))$;

Step 4: **if** $SIG_{stru}(a_k, B, D) \geq 0$

$B \leftarrow B \cup \{a_k\}$;

Go to Step 2;

else

Return B and $\mathbb{T}$;

Step 5: **end**

Table 6
Classification accuracy comparison.

Datasets	HSRM-R	HRS	HE	FS	LS
Hep.	**0.9163**	0.8713	0.8654	0.8838	0.8708
Iono	**0.9288**	0.8917	0.8745	0.9087	0.8860
Horse	**0.9728**	0.9649	0.9649	0.8995	0.8589
Votes	**0.9679**	0.9566	0.9587	0.9449	0.9516
Credit	**0.8333**	0.8087	0.8087	0.8101	0.7217
Zoo	0.9500	0.9500	0.9500	0.8909	**0.9600**
Lym.	**0.8243**	0.8043	0.7976	0.7971	0.7514
Wine	**0.9608**	0.9382	0.9212	0.9497	0.9438
Flags	**0.6500**	0.5832	0.5879	0.6089	0.6079
Autos	**0.7907**	0.7171	0.7121	0.7426	0.6695
Images	**0.8905**	0.8476	0.8571	0.8667	0.8381
Soybean	**0.9253**	0.8828	0.8654	0.8433	0.8434
Vehicle	**0.6714**	0.6655	0.6632	0.6513	0.6312
Tic	**0.9917**	0.8966	0.8883	0.7368	0.7118
German	**0.7030**	**0.7030**	**0.7030**	**0.7030**	**0.7030**
Anneal	**1.0000**	**1.0000**	**1.0000**	0.9978	**1.0000**
Bumps	0.9133	0.9145	0.9149	0.9218	**0.9234**
BHP	**0.9962**	0.9755	0.9568	0.9633	0.9559
DRD	**0.6377**	0.6351	0.6255	0.6255	0.5995
Mushroom	**0.6273**	0.5865	0.5167	0.6233	0.6264
PB	**0.9616**	0.9585	0.9611	0.9607	0.9543
Mean	**0.8625**	0.8358	0.8282	0.8252	0.8099

Liu, Jinfu, **Mingliang Bai**, Na Jiang, and Daren Yu. "A novel measure of attribute significance with complexity weight." Applied Soft Computing 82 (2019): 105543..

Anomaly detection using normal pattern extraction

- Reveal the mapping relationships between measurements and establish the normal pattern of gas turbines.
- Develop a sensitive anomaly detection method.
- The fault detection accuracy outperforms conventional methods.

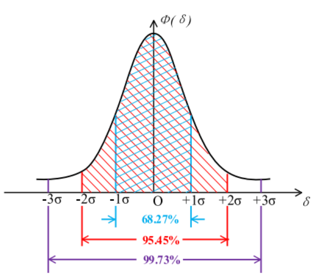

Fig. 7. The diagram of Pauta criterion.

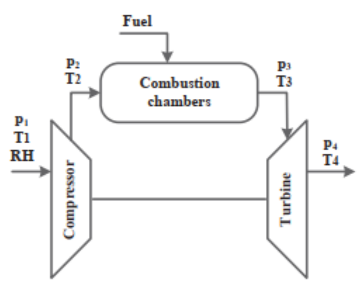

Fig. 4. Typical gas turbine configuration [51]

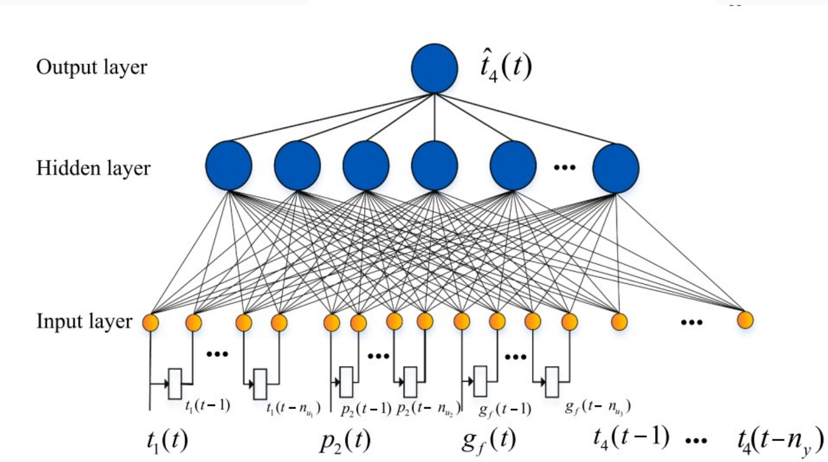

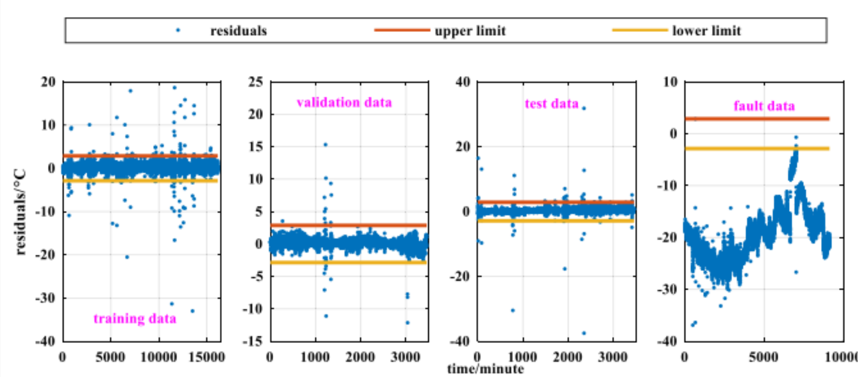

Fig. 18. Detection Performance of NARX Network for Normal Data and Abnormal Data.

Table 4
Comparison of the proposed normal pattern method with other parameter combinations.

Parameter combinations		RMSE			Accuracy of normal data			Accuracy of fault data	Threshold	
Input	Output	Training	Validation	Test	Training	Validation	Test		Lower	Upper
t1	P	10.6824	14.4154	11.3776	0.9883	0.9757	0.9867	0.7545	−32.0423	32.0423
gf	P	10.0075	13.4910	11.9092	0.9886	0.9644	0.9844	0.7580	−60.0233	60.0233
t1 + gf	P	9.8460	12.9202	10.9871	0.9870	0.9734	0.9824	0.5992	−30.3080	30.3080
t1 + gf + p2	P	18.3295	19.9445	15.0754	0.9819	0.9514	0.9844	0.7741	−43.2506	43.2506
t1 + gf + t4	P	14.2387	19.9214	17.5494	0.9900	0.9688	0.9783	0.8148	−42.7170	42.7170
t1 + gf + t4 + p2	P	14.1832	23.6295	16.9098	0.9904	0.9306	0.9751	0.8831	−42.4784	42.4784
t1	p2	0.6979	1.1301	0.8685	0.9919	0.9621	0.9864	0.9177	−2.0935	2.0935
gf	p2	0.7238	1.0714	1.0738	0.9929	0.9858	0.9815	0.8632	−2.1558	2.1558
t1 + gf	p2	1.0616	1.8052	2.0182	0.9905	0.9216	0.9335	0.9624	−2.0432	2.0432
t1 + gf + t4	p2	0.6798	0.9738	1.0373	0.9921	0.9879	0.9748	0.9707	−2.0392	2.0392
t1 + gf + P	p2	0.6908	0.9881	0.9660	0.9924	0.9821	0.9815	0.9611	−2.0720	2.0720
t1 + gf + t4 + P	p2	0.8669	1.5020	0.9968	0.9910	0.9413	0.9783	0.9641	−2.2119	2.2119
t1	t4	0.9211	1.3560	1.4570	0.9929	0.9737	0.9858	0.9305	−2.6784	2.6784
gf	t4	0.8554	1.3428	1.4590	0.9906	0.9528	0.9664	0.9665	−2.5084	2.5084
t1 + gf	t4	1.0988	1.5069	1.6235	0.9903	0.9641	0.9844	0.9889	−2.3483	2.3483
t1 + gf + P	t4	0.9072	1.1357	1.4277	0.9933	0.9902	0.9844	0.9963	−2.7216	2.7216
t1 + gf + P + p2	t4	0.7798	1.0107	2.5318	0.9894	0.9644	0.9690	0.9958	−2.3324	2.3324
Proposed method		0.9747	1.1231	1.4099	**0.9932**	**0.9936**	**0.9867**	**0.9996**	−2.8667	2.8667

Bai M, Liu J, Chai J, et al. Anomaly detection of gas turbines based on normal pattern extraction[J]. Applied Thermal Engineering, 2020, 166: 114664.

Class-imbalanced industrial fault diagnosis

- In fault diagnosis problem, the number of fault samples is few, while the number of normal samples is large, which leads to bad diagnosis accuracy of fault samples.

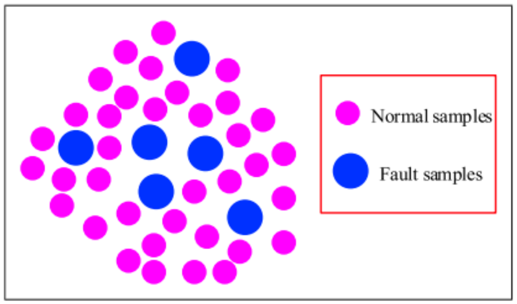

Figure 1. Class-imbalanced data distribution.

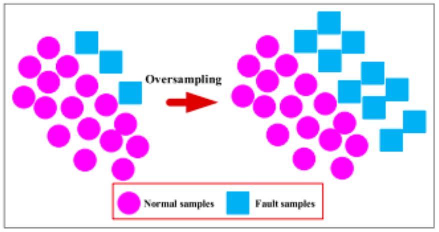

Figure 2. Oversampling.

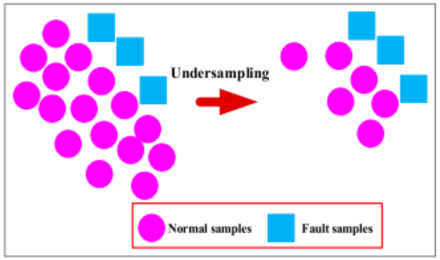

Figure 3. Undersampling.

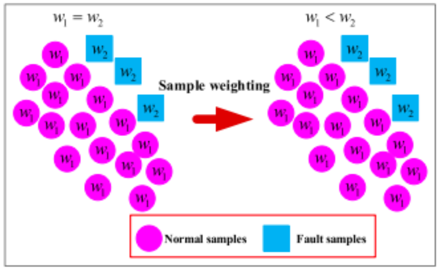

Figure 4. Sample weighting.

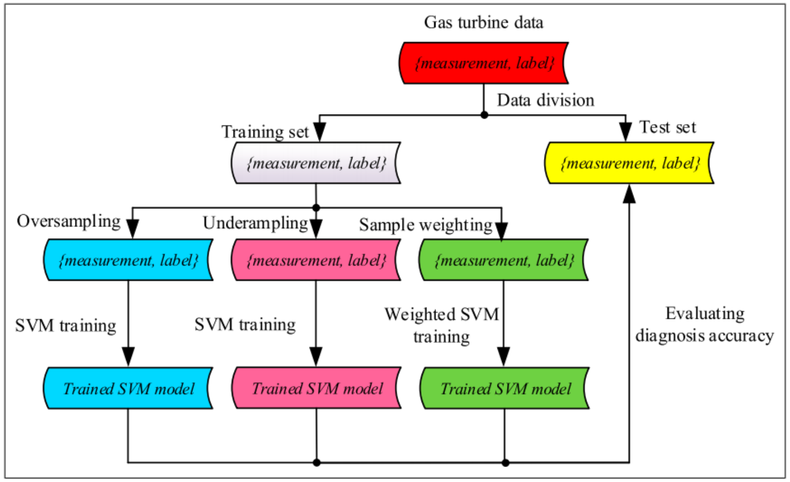

Figure 8. Class-imbalanced gas turbine diagnosis procedure.

Bai Mingliang, et al. "A comparative study on class-imbalanced gas turbine fault diagnosis." Proceedings of the Institution of Mechanical Engineers, Part G: Journal of Aerospace Engineering 237.3 (2023): 672-700.

Class-imbalanced industrial fault diagnosis

- Propose a combined method of oversampling and Focal loss, and the fault accuracy is significantly improved than conventional methods in the class-imbalanced situation.

Table 7. F1-score of Siemens V64.3 gas turbine dataset.

Method		Normal	Fault 1	Fault 2	Fault 3	Fault 4	Fault 5	Mean
Balanced training set		1.0000	1.0000	1.0000	1.0000	1.0000	1.0000	1.0000
Seriously imbalanced training set	Original	0.7982	0.7463	0.7502	0.8041	0.6808	0.6454	0.7375
	ROS	0.9137	0.9719	0.9565	0.9271	0.9732	0.9588	0.9502
	SMOTE	0.9132	0.9727	0.9550	0.9099	0.9732	0.9381	0.9437
	Borderline-SMOTE	0.8612	0.9525	0.7729	0.7989	0.9679	0.6421	0.8326
	RUS	0.8186	0.7403	0.6624	0.7567	0.6791	0.6274	0.7141
	NearMiss	0.5258	0.8869	0.8397	0.6260	0.8789	0.6338	0.7318
	BalanceCascade	0.9091	0.7802	0.7200	0.7721	0.7069	0.5537	0.7403
	EasyEnsemble	0.9243	0.7372	0.7155	0.7615	0.6577	0.6511	0.7412
	RUSBoost	0.8926	0.8766	0.6926	0.7774	0.9033	0.5537	0.7827
	Weighted	0.9011	0.9141	0.9483	0.8665	0.9091	0.8628	0.9003
	Proposed method	**0.9934**	**0.9858**	**0.9784**	**0.9920**	**0.9997**	**0.9916**	**0.9902**

Bai Mingliang, et al. "A comparative study on class-imbalanced gas turbine fault diagnosis." Proceedings of the Institution of Mechanical Engineers, Part G: Journal of Aerospace Engineering 237.3 (2023): 672-700.

Deep transfer learning for fault diagnosis of machines with few fault samples

- Propose the concept of gas turbine group fault diagnosis.
- Deep transfer learning is introduced into the fault detection of gas turbine combustion chambers. Convolutional neural network is pretrained using the data from one data-rich gas turbine and the pretrained convolutional neural network is finetuned for fault detection of another data-poor gas turbine.

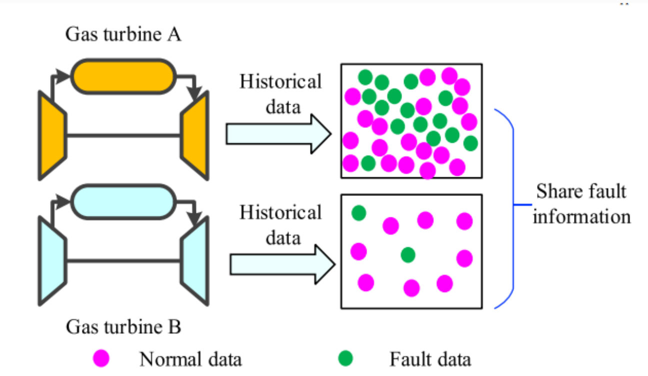

Fig. 3. Fault knowledge sharing in gas turbine group.

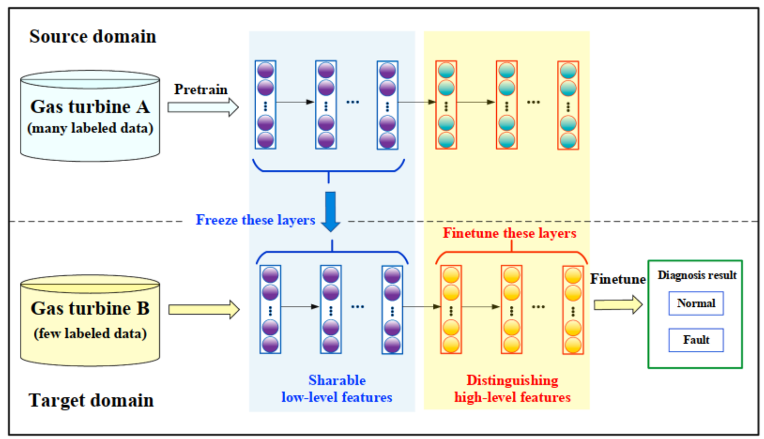

Fig. 10. Architecture of the proposed method.

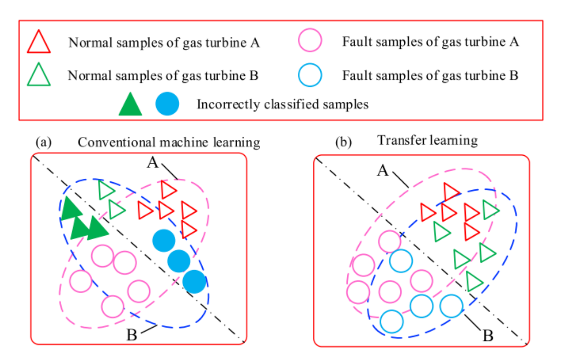

Fig. 4. Conventional machine learning versus transfer learning.

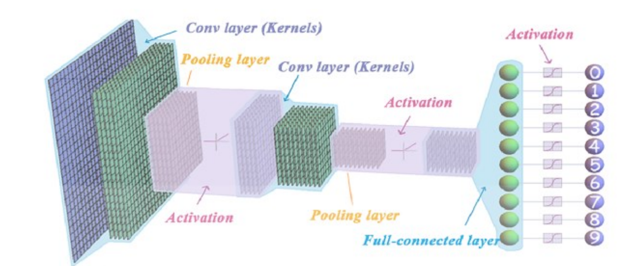

Fig. 6. Typical CNN architecture.

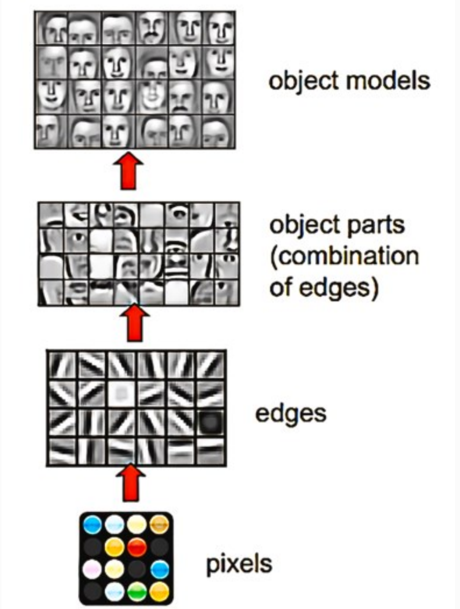

Bai, Mingliang, et al. "Convolutional neural network-based deep transfer learning for fault detection of gas turbine combustion chambers." Applied Energy 302 (2021): 117509.

Deep transfer learning for fault diagnosis of machines with few fault samples

- Through deep transfer learning, fault knowledge is shared between one data-rich gas turbine and another data-poor gas turbine, and the fault detection accuracy of data-poor gas turbine is significantly improved.

Table 9
Classification accuracy of simple mixture.

Method		Overall accuracy	Normal data accuracy	Fault data accuracy
Simple mixture	CNN	0.8225	0.8177	0.8463
	MLP	0.5586	0.5074	0.8147
	SVM	0.9119	0.9453	0.7453
	ELM	0.7137	0.7495	0.5347
	KNN	0.8646	0.9251	0.5621
	NB	0.4975	0.5297	0.3368
	CART	0.7979	0.8312	0.6316
	RF	0.7982	0.8632	0.4737
Proposed method		**0.9502**	**0.9558**	**0.9221**

Table 13
Comparison between deep transfer learning and other simple transfer learning methods.

Method		Overall accuracy	Normal data accuracy	Fault data accuracy
Simple transfer learning methods	TrAdBoost	0.9175	0.9541	0.7347
	DAMLP	0.7025	0.7225	0.6021
	EasyTL	0.8119	0.9528	0.1074
	DAELM-S	0.8298	0.8707	0.6253
Proposed method		**0.9502**	**0.9558**	**0.9221**

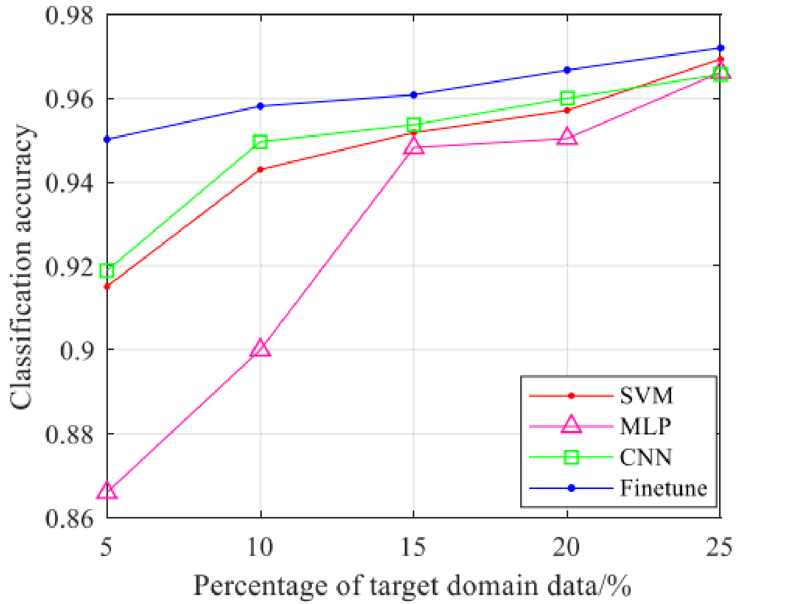

Fig. 15. The change of classification accuracy when target domain data increase.

Bai, Mingliang, et al. "Convolutional neural network-based deep transfer learning for fault detection of gas turbine combustion chambers." Applied Energy 302 (2021): 117509.

Deep transfer learning for fault diagnosis of machines with few fault samples

- Detailed visualization analysis is made to explain why deep transfer learning is effective.

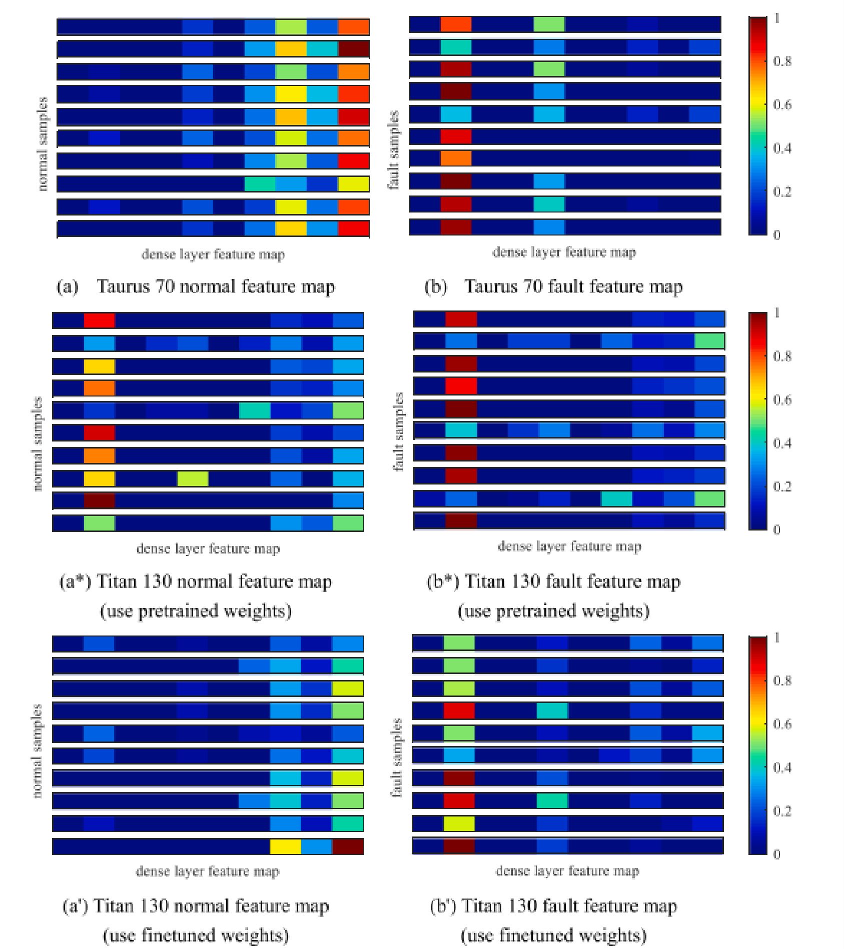

Fig. 20. Feature maps of FC1.

Bai, Mingliang, et al. "Convolutional neural network-based deep transfer learning for fault detection of gas turbine combustion chambers." Applied Energy 302 (2021): 117509.

Multi-angle similarity for remaining useful life prediction

- Propose a new method for remaining useful life prediction with multi-angle similarity.
- Significantly improve the forecast accuracy than conventional methods.

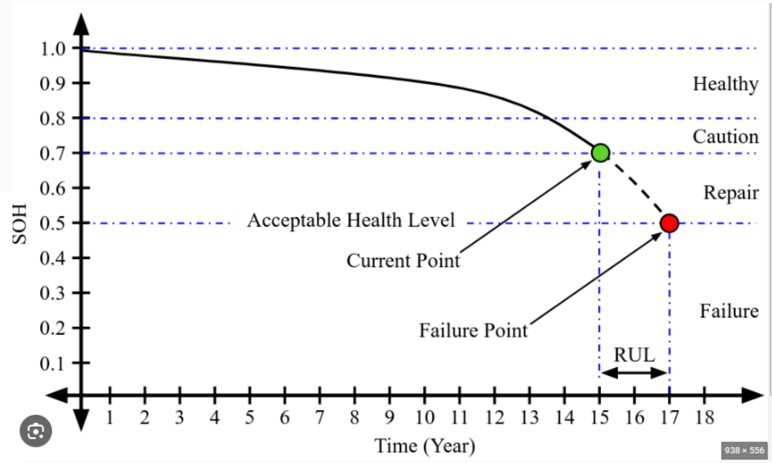

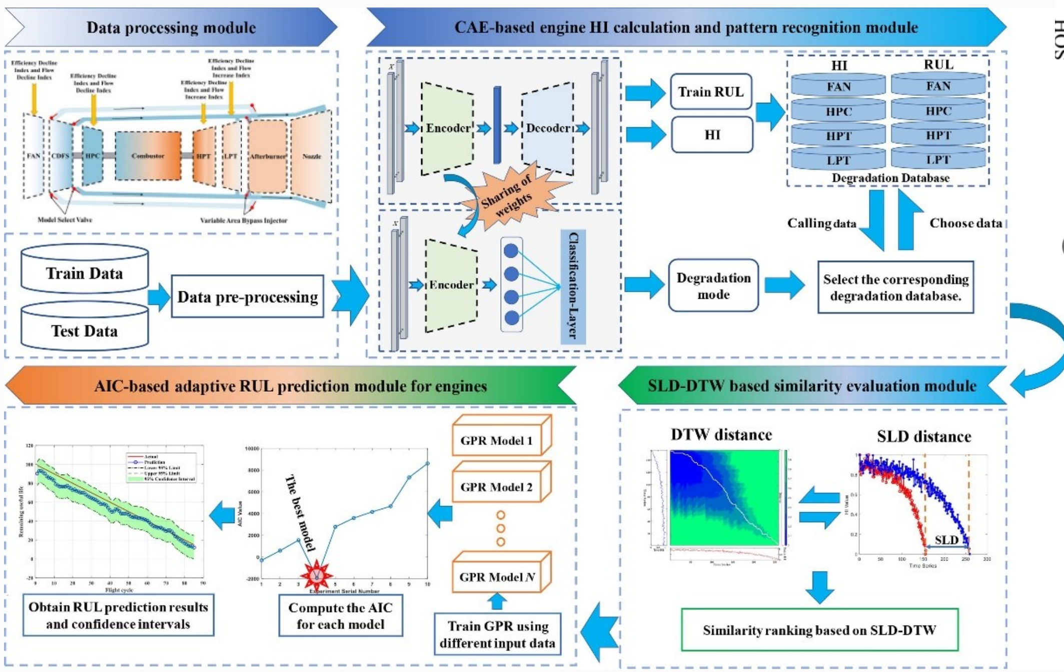

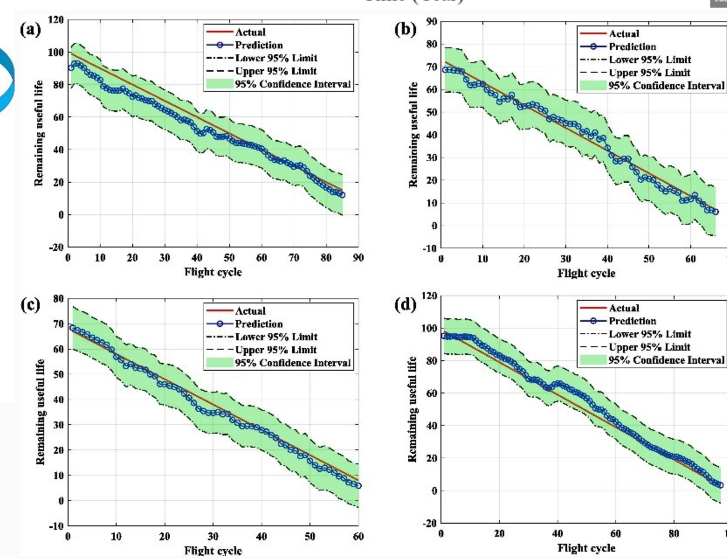

Zhou Z, **Bai M**, Long Z, et al. An adaptive remaining useful life prediction model for aeroengine based on multi-angle similarity[J]. Measurement, 2024, 226: 114082.

Publications

- **28 academic papers, including 25 SCI papers, 1 EI conference paper and 2 papers in Chinese**

1. Bai Mingliang, Yang Xusheng, Liu Jinfu, Liu Jiao, Yu Daren. Convolutional neural network-based deep transfer learning for fault detection of gas turbine combustion chambers [J]. Applied Energy, 2021, 302: 117509.
2. Bai Mingliang, Chen Yunxiao, Zhao Xinyu, Liu Jinfu, Yu Daren. Deep attention ConvLSTM-based adaptive fusion of clear-sky physical prior knowledge and multivariable historical information for probabilistic prediction of photovoltaic power[J]. Expert Systems with Applications, 2022
3. Bai Mingliang, Zhou Zhihao, Li Jingjing, Chen Yunxiao, Liu Jinfu, Zhao Xinyu, Yu Daren. Deep graph gated recurrent unit network-based spatial-temporal multi-task learning for intelligent information fusion of multiple sites with application in short-term spatial-temporal probabilistic forecast of photovoltaic power[J]. Expert Systems with Applications.
4. Bai Mingliang, Liu Jinfu, Chai Jinhua, Zhao Xinyu, Yu Daren. Anomaly detection of gas turbines based on normal pattern extraction[J]. Applied Thermal Engineering, 2020, 166
5. Bai Mingliang, Liu Jinfu, Ma Yujia, et al. Long short-term memory network-based normal pattern group for fault detection of three-shaft marine gas turbine[J]. Energies, 2021, 14(1): 13. (SCI，IF=3.25)
6. Bai Mingliang, Liu Jinfu, Long Zhenhua, Jing Luo, Yu Daren. A comparative study on class-imbalanced gas turbine fault diagnosis [J]. Proceedings of the Institution of Mechanical Engineers, Part G: Journal of Aerospace Engineering
7. Bai Mingliang Zhou Zhihao, Chen Yunxiao, Liu Jinfu, Yu Daren. Accurate four-hour-ahead probabilistic forecast of photovoltaic power generation based on multiple meteorological variables-aided intelligent optimization of numeric weather prediction data[J]. Earth Science Informatics.
8. Bai Mingliang, Chen Yunxiao, Zhou Zhihao, Long Zhenhua, Liu Jinfu, Yu Daren. Deep attention convolutional neural network-based adaptive multi-source information fusion for accurate short-term photovoltaic power forecast[C]. 2023 IEEE/ PES Innovative Smart Grid Technologies Europe (ISGT EUROPE)
9. 白明亮，张冬雪，刘金福，刘娇，于达仁. 基于深度自编码器和支持向量数据描述的燃气轮机高温部件异常检测[J]. 发电技术. 2021
10. Liu Jinfu, Bai Mingliang, Jiang Na, Yu Daren. A novel measure of attribute significance with complexity weight[J]. Applied Soft Computing, 2019, 82
11. Liu Jinfu Bai Mingliang, Jiang Na, Yu Daren. Structural risk minimization of rough set-based classifier[J]. Soft Computing, 2019, 24(3)
12. Liu Jinfu, Bai Mingliang, Jiang Na, et al. Interclass Interference Suppression in Multi-Class Problems[J]. Applied Sciences, 2021, 11(1): 450.
13. Liu Jinfu, Bai Mingliang, Long Zhenhua, et al. Early Fault Detection of Gas Turbine Hot Components Based on Exhaust Gas Temperature Profile Continuous Distribution Estimation[J]. Energies, 2020, 13(22): 5950.
14. Zhao Xinyu, Bai Mingliang, Yang Xusheng, Liu Jinfu, Yu Daren, Chang Junta, Short-term probabilistic predictions of wind multi-parameter based on one-dimensional convolutional neural network with attention mechanism and multivariate copula distribution estimation[J]. Energy, 2021.
15. Long Zhenhua, Bai Mingliang, Ren Minghao, Liu Jinfu, Yu Daren. Fault detection and isolation of aeroengine combustion chamber based on unscented Kalman filter method fusing artificial neural network[J]. Energy.
16. Zhou Zhihao, Bai Mingliang, Long Zhnehua, Liu Jinfu, Yu Daren. An adaptive remaining useful life prediction model for aeroengine based on multi-angle similarity[J]. Measurement.
17. Zhou Guowen, Bai Mingliang et al. Multi-objective station-network synergy planning for regional integrated energy system considering energy cascade utilization and uncertainty. Energy Conversation and Management.
18. Zhou Guowen, Bai Mingliang, Zhao Xinyu, Li Jiajia, Liu Jinfu, Yu Daren, Study on the distribution characteristics and uncertainty of multiple energy load patterns for building group to enhance demand side management[J]. Energy and Buildings
19. Chen Yunxiao; Bai Mingliang; Zhang Yilan; Liu Jinfu, Yu Daren. Proactively selection of input variables based on information gain factors for deep learning models in short-term solar irradiance forecasting[J]. Energy
20. Yang Xusheng, Bai Mingliang, Liu Jinfu, Liu Jiao, Yu Daren. Gas path fault diagnosis for gas turbine group based on deep transfer learning [J]. Measurement, 2021: 109631. (SCI，IF=5.13)
21. Li Xingshuo, Liu Jinfu, Bai Mingliang, et al. An LSTM based method for stage performance degradation early warning with consideration of time-series information[J]. Energy, 2021, 226: 120398.
22. Chen Yunxiao, Bai Mingliang, Zhang Yilan, Liu Jinfu, Yu Daren. Error revision during morning period for deep learning and multi-variable historical data-based day-ahead solar irradiance forecast: towards a more accurate daytime forecast[J]. Earth Science Informatics, 2023: 1-23.
23. Chen Yunxiao, Bai Mingliang, Zhang Yilan, Liu Jinfu, Yu Daren. Multivariable space-time correction for wind speed in numerical weather prediction (NWP) based on ConvLSTM and the prediction of probability interval [J]. Earth Science Informatics, 2023: 1-23.
24. Liu Jinfu, Long Zhenhua, Bai Mingliang, et al. A Comparative Study on Fault Detection Methods for Gas Turbine Combustion Systems[J]. Energies, 2021, 14(2): 389.
25. Zhu Linhai, Liu Jinfu, Ma Yujia, Bai Mingliang, Zhou Weixing, Yu Daren. Gas turbine system identification using a bilayer equilibrium manifold expansion model[J]. Aircraft Engineering and Aerospace Technology.
26. Long Zhenhua, Zhou Zhihao, Qin Zizhen, Luo Jing, Bai Mingliang, Liu Jinfu, Yu Daren. Research on active modulation of gas turbine cooling air flow[J]. Applied Thermal Engineering, 2023: 120874.
27. 李兴朔，刘金福，白明亮，李献领，刘东航，颜培刚，于达仁．基于非线性有源自回归模型的船用凝汽器故障早期预警[J]．推进技术
28. Long Z, Zhou Z, Suo P,. Yao P, Bai M, Liu J, Yu D, Gas turbine circumferential temperature distribution model for the combustion system fault detection[J]. Engineering Failure Analysis, 2024: 108032.

THANK YOU！